

INFLUENCE MECHANISM OF LOCAL AIR FILM HOLES BLOCKAGE ON COOLING EFFICIENCY OF TURBINE BLADES

by

Miao GONG*, Wen HUANG, Yuanhang SHEN, and Cunyuan MA

Institute of Aviation Engineering, Civil Aviation University of China, Tianjin, China

Original scientific paper

<https://doi.org/10.2298/TSCI230905012G>

In order to explore the cooling air film damage mechanism of aero-engine turbine blades in different blockage states, the air film cooling efficiency, outlet temperature and flow rate variations have been studied in three typical positions with different blockage ratios. The results show that the blockage of the air film holes decreases the air film cooling efficiency in the downstream region of the outlet boundary, and the decreasing amplitude increases non-linearly. When the temperature of the air film hole is lower than 1100 K, the cross-section of the air film gradually flattens out and the air film becomes thinner with the increase of the blocking ratio. When the blockage is in inlet position A, and $B = 0.8$, the influence on cooling efficiency of the air film performs most apparently. Moreover, when the cooling efficiency is near $x/d = 1$, the decreasing amplitude of efficiency reaches more than 7%. When the cooling efficiency is near $x/d = 4$, the decreasing amplitude of efficiency reaches more than 10%. In these two conditions, the effective protective air film area is the smallest, and the angle between the high temperature mainstream and the cooling fluid is the smallest, and the cooling fluid and the high temperature mainstream are the weakest in terms of resistance. Experiments on the effect of cooling fluid coverage of static blades have been conducted, and the results indicate that in the case of local air film holes blockage, the trend of damage degree of the cooling flow field is in good consistency with the analyzed results of the numerical model.

Key words: turbine blade, air film hole, blockage, air film cooling, heat transfer

Introduction

The components of aviation air turbine engines have worked in extreme conditions of high temperature, high pressure, and high speed rotation for prolonged period [1]. To reduce the risk of engine failure, air film cooling is widely applied to aviation engines as this technique can significantly cool the surface of the protected components and the blades. However, when an aviation turbine engine operates with heavy pollution or other contaminant, the fine particles inhaled by the engine will deposit on the blade surface, forming deposition blockages in the cooling structure of the blade. This factor can lead to blockages in the inner air film hole, resulting in a reduction of cooled air coverage and output of air film holes [2]. This deterioration can give a sharp rise in turbine blade surface temperature, leading to turbine blade fracture [3]. Recent progress has been made in predicting particle deposition on the guide vane of a plated nozzle through deposition experiments and numerical calculations [4, 5]. The results show that particles are mainly deposited on the front and pressure surfaces and the deposition efficiency increases with the increase of wall temperature. There is a potential risk of complete air film

* Corresponding author, e-mail: mgong@cauc.edu.cn

hole blockage, which changes the flow and heat transfer characteristics of film cooling. The maximum reduction rate of regional average efficiency caused by blockage can reach above 90%, and when the blocking ratio and the blow ratio are relatively larger, the flow coefficient and aerodynamic loss increase significantly [6, 7].

The study conducted by Li *et al.* [8] showed that blocking air film holes make heat transfer coefficient distribute unevenly and weaken air film cooling performance. Huang *et al.* [9] conducted a numerical study on the local blockage of air film holes on a flat plate and found that the local blockage at the leading edge of the outlet end of the air film hole can improve the adiabatic film cooling efficiency in the downstream region of the air film hole, while blockages at the inlet end and middle of the hole exert much less influence to its cooling efficiency. Zhou and Zhang [10] analyzed the influence of blocking position and ratio on the cooling efficiency of the blade pressure surface to the blade pressure surface through numerical simulation. In contrast, Pu *et al.* [11] studied the effect of air film cooling efficiency on concave surface when the holes are blocked in accordance with the size of the air film holes, and found that the cooling efficiency and the area covered by the cooling fluid significantly decreases because of the blockage Sundaram *et al.* [12] discovered that deposition near the hole outlet could improve the cooling effect of the leading edge, but the cooling effect worsened with the rising height of deposition. Yang *et al.* [13] demonstrated that the pressure side of the blade is more sensitive to the deposition blockage of air film holes in terms of cooling effect and film coverage area.

In accordance with various studies, the efficiency of air film cooling is influenced by factors such as blocking ratio, air blow ratio, and density flow rates (DFR). Guo *et al.* [14] found that the air film cooling efficiency was significantly affected by the change of the air blow ratio in the case of low and medium blockage ratio, while in the case of high blockage ratio, the impact on the air film cooling efficiency caused by the change of the air blow ratio dilutes. Whitfield *et al.* [15] observed that blockage with 0.5 times the aperture could reduce the film cooling efficiency by up to 75%. The height and location of the blockage were also factors affecting the effect of film cooling. Through experiments, Wei *et al.* [16] investigated the effects of different DFR on air film cooling and concluded that, as DFR increases, the cooling effect on the induction plate improves. Zhang *et al.* [17] found that the average film efficiency of the surface decreased significantly when the blocking ratio was high. Finally, several studies showed that large blockage in the hole reduced the area and uniformity covered by the coolant, leading to a significant decline in the effect of air film cooling [18-20]. Overall, blockage makes the flow and heat transfer mechanism of film cooling more complicated and puts forward higher requirements for the design and evaluation of film cooling [21].

Huang *et al.* [22] also investigated the effects of cone blocking on flow coefficient and film efficiency, finding that blocking in the hole reduces the flow coefficient and decreases efficiency in all forms except leading edge orifice blocking. Furthermore, Jovanovic *et al.* [23-25] found that the blocking position of the air film hole had different impacts on cooling characteristics depending on the blowing ratio, with blocking in the hole even improving cooling effects in some cases. The size and position of blockages in air film hole channels can be unpredictable, making the study of blocking characteristics and their influence on flow and cooling effects crucial for optimizing air film cooling designs and evaluating cooling performance degradation [26]. It is necessary to thoroughly investigate this complex issue to ensure the health and longevity of turbine blades.

In accordance with the aforementioned literature, air film hole blockage has been researched both domestically and internationally, and the current focus is mainly on the outlet part. However, in complex aero-engine working conditions, the size and position of air film hole plug are random, and the impact on air film cooling is extremely complicated. As a result,

the current work aims to analyze how the local air film hole blockage on the aero-engine turbine blade influences the cooling efficiency of the blade surface cooled by building spherical blocking objects with three radii and by building aero-engine turbine blade air film cooling models in three distinctive blocking positions. Furthermore, through varying the blocking ratios and the blocking positions, the fact of blade's air film holes can be further approached, taking further steps to study the complicated influences on air film holes caused by blockage. Finally, the current study provides a better understanding of the impact of blockages in different sizes and positions on the turbine blade film cooling, which helps to judge the airworthiness of turbine blades and improve flight operation safety.

Computational governing equation

The SST model is used to investigate issues related to air film cooling efficiency [27]. eq. (1) is the RANS equation:

$$\rho \frac{\partial \mathbf{u}}{\partial t} + \rho \mathbf{u} \nabla \mathbf{u} = -\nabla p \mathbf{I} + \nabla \left[\mu (\nabla \mathbf{u} + (\nabla \mathbf{u})^T) - \frac{2}{3} \mu (\nabla \mathbf{u}) \mathbf{I} \right] + \mathbf{F} \quad (1)$$

Flow problems need follow the mass conservation law. The continuity equation:

$$\frac{\partial \rho}{\partial t} + \nabla (\rho \mathbf{u}) = 0 \quad (2)$$

Since this study focuses on weakly compressible flow, $\partial \rho / \partial t = 0$, $\nabla (\rho \mathbf{u}) = 0$, the viscous force term in eq. (1): $(2/3)\mu(\nabla \mathbf{u})$ is equal to 0:

$$\rho (\mathbf{u} \nabla) \mathbf{u} = \nabla \left[-p \mathbf{I} + \mu (\nabla \mathbf{u} + (\nabla \mathbf{u})^T) \right] + \mathbf{F} \quad (3)$$

The numerical simulation uses the fluid-structure coupled heat transfer model, and the conjugate heat transfer interface combines the heat equation with the turbulent N-S equation.

The heat transfer equation in the fluid domain:

$$\rho C_p (\mathbf{u} \nabla T) + (\nabla \mathbf{q}) = Q \quad (4)$$

The heat transfer equation in the solid domain:

$$(\nabla \mathbf{q}) = Q + Q_{\text{ted}} \quad (5)$$

At the non-isothermal flow interface, the viscous heat generation term cannot be neglected and the term is controlled by:

$$Q_{\text{vd}} = \boldsymbol{\tau} : \nabla \mathbf{u} + Q_{\text{turb}} \quad (6)$$

The heat equation of the fluid domain:

$$\rho C_p \mathbf{u} \nabla T = -(\nabla \mathbf{q}) + \boldsymbol{\tau} : \mathbf{S} - \frac{T}{\rho} \frac{\partial \rho}{\partial T} \mathbf{u} \nabla p + Q \quad (7)$$

The thermal equation of the solid domain and physical interface:

$$\rho C_p \mathbf{u} \nabla T = -(\nabla \mathbf{q}) + Q + Q_{\text{ted}} \quad (8)$$

Numerical simulation

Local blockage geometry model

The blocking ratio is calculated:

$$B = \frac{4A_{b,\text{max}}}{\pi d^2} \quad (9)$$

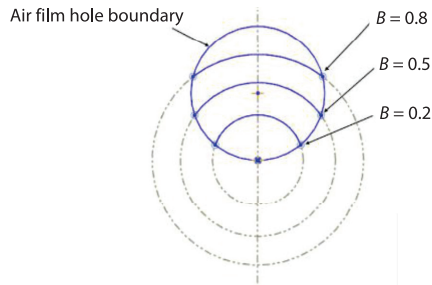


Figure 1. Maximum cross-section of clog

where $A_{b,max}$ is the maximum cross-sectional area of the blockage on the plane perpendicular to the axis of the air film hole, as shown in fig. 1.

In accordance with the formula of the blocking ratio, the numerical value of the blocking ratio represents the ratio of the maximum cross-section of the blockage on the plane perpendicular to the axis of the hole to the cross-section of the air film hole on the same plane. Changing the diameter of the blocking material makes the blockage in the hole reach the corresponding blocking ratio. The diameter of the air film hole is 0.5 mm.

The data in tab. 1 shows the diameters of hemispherical blockages in different blocking ratios. Figure 2 presents the micrograph of the air film hole blocking at the same temperature and the cross-section of three different blocking ratios of the turbine blade air film hole blocking model.

Table 1. Diameters of different blocking ratios

Ratio of blockage	Diameter of hemispherical blockage [mm]
0.2	0.34
0.5	0.58
0.8	0.79

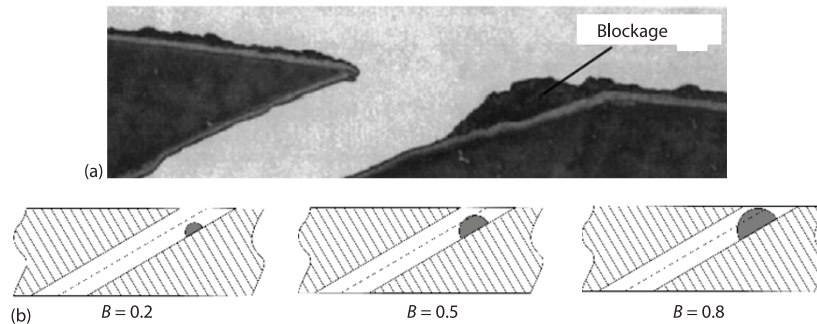


Figure 2. Air film hole blocking model; (a) SEM photo of blockage [28] and (b) three sizes of blockage in the air film hole

The selected locations for constructing local blocking holes on the blade are shown in fig. 3. In fig. 3(b), Position 1 near the blade surface and Position 2 near the inner flow passage are highlighted. In order to facilitate the discussion of the results, the Position 1 of the blockage at the inlet end is named as the inlet end Position 1, and the four air film holes at the bottom of the pressure surface of the blade are selected to construct a local blockage model. Figure 4 shows the 3-D models of hemispherical plug in different positions in the air film holes ($B = 0.2$). The center of the hemispherical blockage is at the edge of the air film hole, and blocking ratio B , changes by changing the diameter of the hemispherical blockage. The blockages are set in the outlet of air film hole 1 (outlet Position 1), the outlet of air film hole 2 (outlet Position 2), and the inlet of air film hole A (inlet Position A), respectively. In the blockage model with the outlet position of the air film hole 1, the boundary of the blockage is not directly in contact with the boundary of the hole and blade (the exit boundary of the air film hole). In the blockage model

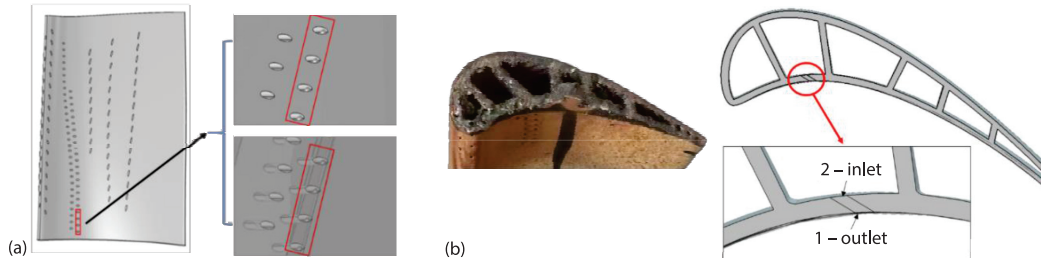


Figure 3. Schematic diagram of blade runner and air film hole; (a) location of the blocked hole and (b) blade inner flow path and geometry model runner

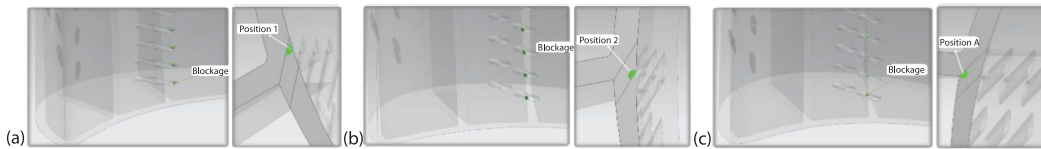


Figure 4. Air film hole local blocking scheme ($B = 0.2$); (a) outlet Position 1, (b) outlet Position 2, and (c) inlet Position A

with outlet Position 2 and inlet Position A, the boundary of the blockage is directly in contact with the intersection boundary of the hole and blade.

Three variable parameters 0.2, 0.5, and 0.8 of blocking ratio B are taken. The higher the blocking ratio value, the more serious the blocking degree of the air film hole. In consideration of the comprehensive comparison and analysis of the simulation results, three different blocking rates are preset in each area of the four selected blockage positions. The results are compared with the numerical simulation results of the blocking rate $B = 0$ (main comparative reference).

Parameter definitions and boundary conditions

Local blocking is simulated for each model with a blowing ratio $M = 1.5$. Except the inlet and outlet, the walls of the mainstream passage of the blade are set in adiabatic non-slip boundary conditions. The turbulence intensity of the mainstream is 5%. The inlet temperature of the mainstream is $T_g = 1500$ K, the flow rate is set to $v_g = 20$ m/s, the inlet temperature of the cooling passage is $T_c = 750$ K, and the density ratio is $D_R = 2.0$. The outlet is set as the pressure outlet, and the pressure is constant $1.013 \cdot 10^5$ Pa. In order to ensure that the blow ratio of the air film holes is 1.5, the flow velocity at the outlet of the air film hole should be calculated at first from the mainstream flow velocity and blow ratio, and then the flow velocity at the entrance of the internal flow passage should be calculated based on the principle that the volume of gas entering the flow passage and the volume of gas-flowing out of the air film holes connected by each flow passage should be equal.

The inner runner inlet is at the bottom of the blade. In order to simplify the model, the influence of the blockage on thermal conductivity is not considered, thereby the blockage and blade are connected as a whole, and the blockage material is the same as the blade material.

The blowing ratio M :

$$M = \frac{\rho_c v_c}{\rho_g v_g} \quad (10)$$

The density ratio D_R :

$$D_R = \frac{\rho_g}{\rho_c} \quad (11)$$

The air film cooling efficiency:

$$\eta = \frac{T_g - T_{aw}}{T_g - T_c} \quad (12)$$

Turbulence model adopts SST model. The computational model convergence criterion is $1 \cdot 10^{-6}$ for the initialized relative tolerance of wall distance and $2 \cdot 10^{-3}$ for the steady-state energy equation when solving the continuity equation, linear momentum equation and the SST model equation. Before starting the numerical model study, an independence analysis of the mesh is required to ensure the accuracy of the calculation.

The dimensionless position of the flow direction is divided in such a way that the intersection-line of the pressure and suction surfaces of the blade is taken as the centerline, and the pressure and suction surfaces are flattened into a plane. The co-ordinate value of pressure surface is positive, and that of suction surface is negative, and the distance from the centerline to the edge of the blade is 1 unit as shown in fig. 5. Figure 6 shows the comparison diagram of the average span wise film cooling efficiency under different grid numbers when the blade air film cooling characteristics are studied at $v_g = 20$ m/s and $M = 1.25$. When the total number of grids is $1.85 \cdot 10^6$, the changes are basically identical with those when the total number of grids is $2.19 \cdot 10^6$, and the calculated results change less than 5%, which is considered to meet the requirements of grid independence. When the total number of grids is $2.54 \cdot 10^6$, the maximum error is more than 10%. Therefore, a model with a calculated grid number of $2.20 \cdot 10^6$ is finally adopted in the study to analyze the air film cooling characteristics and flow field.

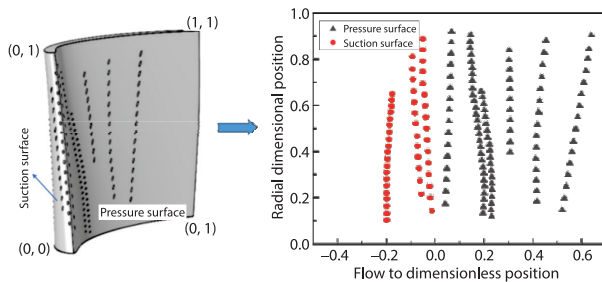


Figure 5. Flow direction dimensionless location description chart

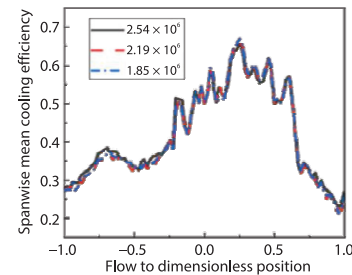


Figure 6. Average span wise film cooling of blocking

The minimum mesh size of internal runner and air film hole is 0.01 mm. The minimum mesh size of blade is 0.001 mm. The minimum mesh size of the mainstream passage is 4 mm, and the maximum cell growth rate is 1.5. Besides, the maximum mesh sizes are 20 mm in the meshing of all parts. Whether the minimum mesh meets the requirements of the turbulence numerical model. Due to the different location and size of the blockage in different models, there will be some differences in the number of grids in each model. In summary, the number of grid cells in all models is around $2.20 \cdot 10^6$, and the average cell mass of all models is greater than 0.64 when the skewness is used to measure the grid quality.

Analysis of the effect of blocking on air film cooling

Effect of blocking on the cooling efficiency of air film

Figure 7 shows the influence of different blocking ratios in different positions on the cooling efficiency of the air film when the blowing ratio is 1.5. When the air film holes are blocked, the cooling efficiency of the air film in the downstream region of the outlet boundary of the air film holes decreases. The blockage of the air film holes changes the state of the flow field for the formation of the protective air film, leading to a shortening of the extended protection distance of the cooling air, which is a similar trend to the phenomenon described in [7].

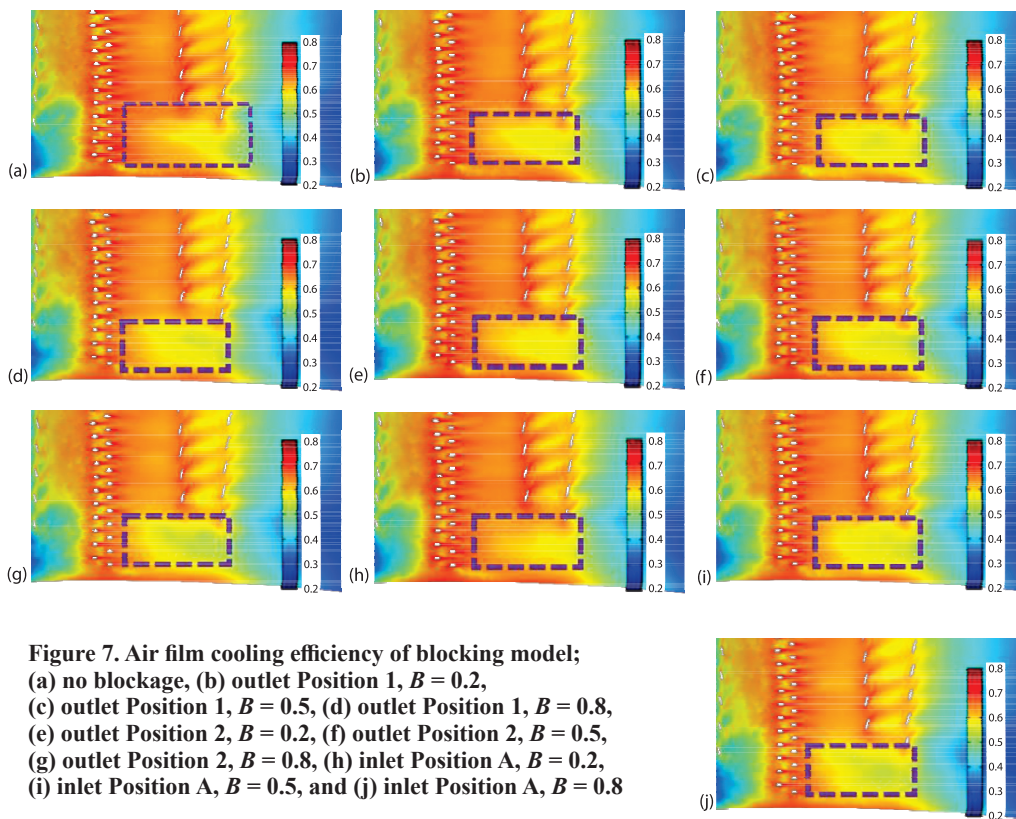


Figure 7. Air film cooling efficiency of blocking model;
 (a) no blockage, (b) outlet Position 1, $B = 0.2$,
 (c) outlet Position 1, $B = 0.5$, (d) outlet Position 1, $B = 0.8$,
 (e) outlet Position 2, $B = 0.2$, (f) outlet Position 2, $B = 0.5$,
 (g) outlet Position 2, $B = 0.8$, (h) inlet Position A, $B = 0.2$,
 (i) inlet Position A, $B = 0.5$, and (j) inlet Position A, $B = 0.8$

As shown in fig. 7, the larger the blocking ratio B , the greater the impact on the cooling efficiency of the air film, resulting in a decrease in the efficiency of local areas. The effect of blockage is weakest when the blockage is in outlet Position 1. In inlet Position A, the cooling efficiency of the air film decreases significantly. When the blocking ratio $B = 0.8$, different positions have the most obvious effect on the cooling efficiency of the air film, and the cooling efficiency in inlet Position A performs best. At other blocking ratios, the position of the blockage has little influence on the cooling efficiency of the air film. To conclude, when the blocking ratio $B = 0.8$ and the blockage is located in inlet Position A, the effect on the cooling efficiency of the air film is the greatest, and the decrease of efficiency is most obvious.

With the increase of the blocking ratio, a large-scale asymmetric inverse vortex will be formed on the blade surface, which is formed by the interaction between the coolant and

the mainstream of the boundary-layer. The reverse vortex has two important negative effects. First is to entrap hot gas under the jet, which makes the hot gas to be close to the blade surface, reducing the cooling efficiency of the air film. Second is to induce the cooling air film away from the wall so that the mixing of the cooling flow field and the mainstream increases, and the cooling efficiency of the air film decreases. When the blocking ratio increases, the size of the reverse vortex increases and the transverse distance near the wall decreases, and the film of the coolant flux cannot effectively get close to the blade surface to form a cooling barrier.

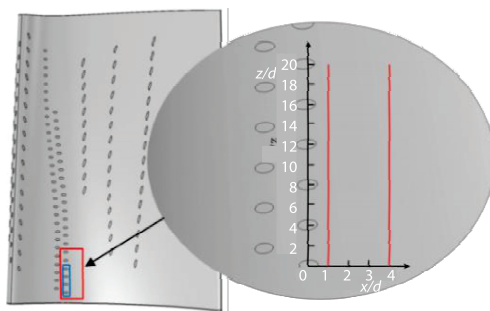
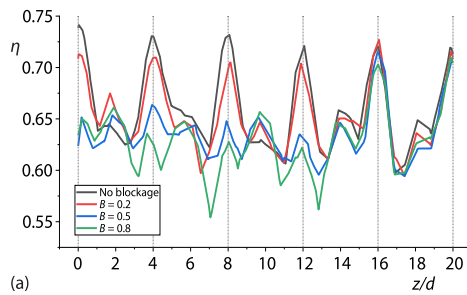
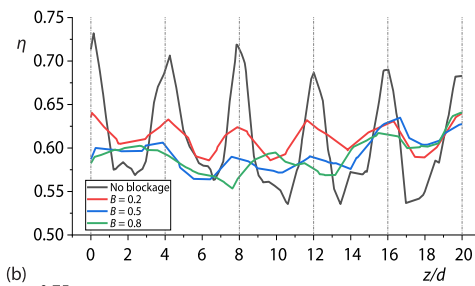


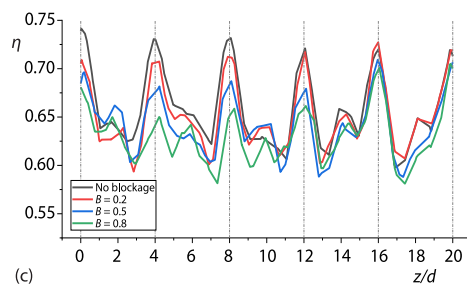
Figure 8. Diagram of air film cooling efficiency of air film variation at $x/d = 1$ and $x/d = 4$; (a) cooling efficiency of air film detection location diagram, (b) $x/d = 1$, outlet Position 1, (c) $x/d = 4$, outlet Position 1, (d) $x/d = 1$, outlet Position 2, (e) $x/d = 4$, outlet Position 2, (f) $x/d = 1$, inlet Position A, and (g) $x/d = 4$, inlet Position A



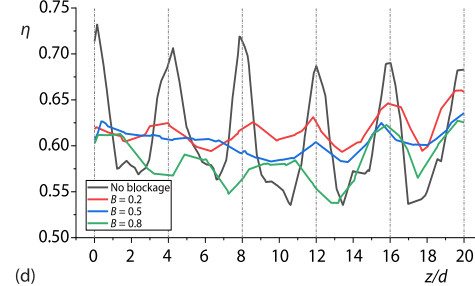
(a)



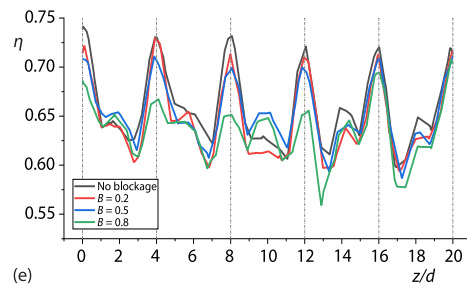
(b)



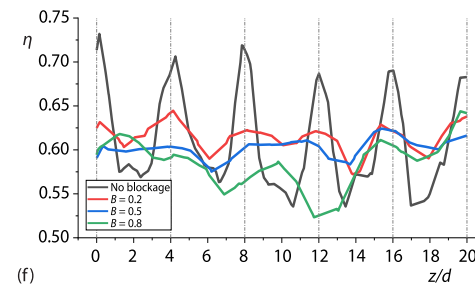
(c)



(d)



(e)



(f)

The detection position of the cooling efficiency of blade air film is shown in fig. 8(a). The downstream region of the blocking hole is selected as the research object, and the blade pressure surface is flattened on a plane. The intersection point between the air film hole axis at the bottom of the third column of the pressure surface and the blade surface was taken as the origin point, and the direction of the upward arrangement along the air film hole is the longitudinal axis. The two red lines in the co-ordinate system are the routes to detect the cooling efficiency of air film, with a length of 10 mm and the corresponding horizontal co-ordinates are $x/d = 1$ and $x/d = 4$. In order to facilitate observation, in figs. 8(b)-8(g), z/d is taken as the horizontal co-ordinate, the overall cooling efficiency of air film is taken as the vertical co-ordinate, and 0, 4, 8, and 12 on the horizontal axis are the corresponding positions of blocking holes.

Figure 8 shows that in the range of z/d from 0-14, the unblocked air film cooling efficiency at $x/d = 1$ is 72.55%, and that of $x/d = 4$ is 69.50%. Figures 8(b)-8(f) shows that when $x/d = 1$, z/d is in the range of 0-14, the cooling efficiency is affected by the blocking ratio. In combination with tab. 2, it can be seen that in the same position, the reduction degree of cooling efficiency shows a non-linear change with the increase of blocking ratio. At a small blocking ratio ($B \leq 0.2$), the effect of blocking in different positions on the cooling efficiency is similar, less than 2%. At the same time, it can also be seen from fig. 8(e) that under a small blockage ratio, the cooling efficiency of the blockage in outlet Position 2 is more evenly distributed, and the probability of local overheating damage is relatively small, which is consistent with the research views of literature [29]. With the increase of the blocking ratio, the blockage in inlet Position A has more obvious influence on the cooling efficiency of air film. When $B = 0.8$, the decrease reaches to 7.29%. Moreover, it can be concluded from the cloud map of cooling efficiency that the damaged area of the downstream region of cooling air film generated by the blockage in inlet Position A has strong non-uniformity, which is easy to cause local thermal stress damage.

As compared from tab. 2 and figs. 8(c)-8(g), when $x/d = 4$, z/d is in the range of 0-14, the cooling efficiency is affected by the blocking ratio. The results show that the decrease of cooling efficiency at $x/d = 4$ is more significant than that at $x/d = 1$, and the influence rules of both are similar. When $x/d = 4$, in the same position, the decrease of cooling efficiency becomes sharper with the increase of blocking ratio. In the $x/d = 4$ downstream region of the blocking hole, the cooling efficiency of the air film is significantly reduced by the blockage in three positions, and the reducing degree is similar. Combined with tab. 2, only when $B = 0.2$, the influence of the three blocking states on the cooling efficiency exceeds 6%, and when $B = 0.8$, the cooling efficiency decreases by over 10%. The blockage in inlet Position A causes the most serious damage to the cooling efficiency of the air film.

Table 2. The $x/d = 1$, the average reduction of cooling efficiency at the outlet of the blocking hole

Blocking position	$B = 0.2$	$B = 0.5$	$B = 0.8$
Inlet Position 1	1.06%	2.20%	5.01%
Outlet Position 2	1.12%	3.52%	5.49%
Inlet Position A	1.55%	6.05%	7.29%

Table 3. The $x/d = 4$, the average reduction of cooling efficiency at the outlet of the blocking hole

Blocking position	$B = 0.2$	$B = 0.5$	$B = 0.8$
Inlet Position 1	6.46%	8.67%	10.54%
Outlet Position 2	6.52%	9.02%	10.01%
Inlet Position A	6.99%	8.78%	11.38%

Effect of blocking position on outlet temperature

Figure 9 shows the temperature cloud diagram of the cross-section of the blade and the inner and outer flow channels of the blade, which is perpendicular to the surface of the blade. The temperature distribution cloud diagram in unblocked condition is shown in fig. 9(a), and

the temperature distribution cloud diagram in unblocked condition is shown from figs. 9(b)-9(k). Comparison of figs. 9(a) and 9(b) shows that the temperature in the region between the circled blade boundary and the temperature color in fig. 9(b) is lower than 1100 K, which is the protective air film created by the air-flowing out of the air film holes.

It can be seen that the area and covering length of the downstream area with temperature below 1100 K decrease with the increase of blocking ratio. In the case of A certain blocking ratio, the relationship between the effective air film coverage area is outlet Position 1 > outlet Position 2 > inlet Position A. In inlet Position A, when the blocking ratio $B = 0.8$, the length and area of the cooling air film are most affected.

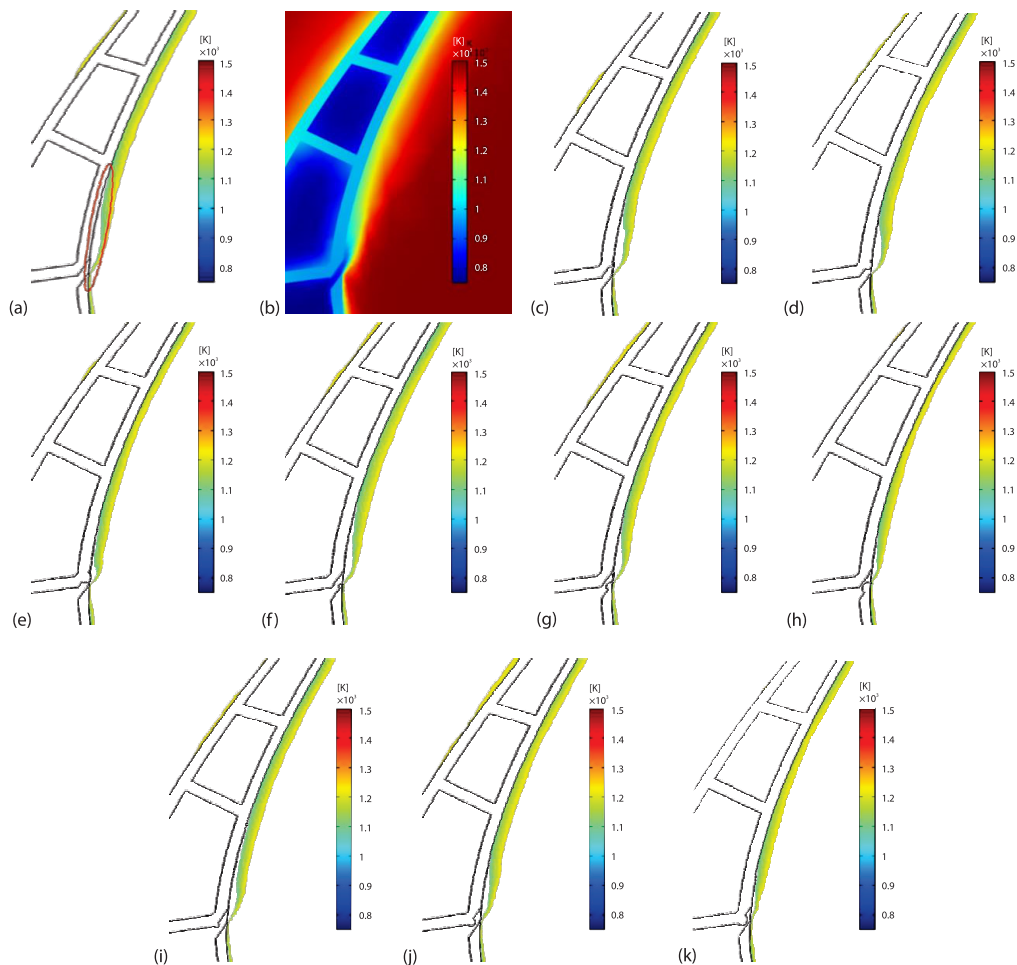


Figure 9. Temperature cloud of flow cross-section on the axis of blocking hole;

- (a) no blockage, (b) no blockage (1100~1240 K),
 (c) outlet Position 1, $B = 0.2$, (d) outlet Position 1, $B = 0.5$,
 (e) outlet Position 1, $B = 0.8$, (f) outlet Position 2, $B = 0.2$,
 (g) outlet Position 2, $B = 0.5$, (h) outlet Position 2, $B = 0.8$,
 (i) inlet Position A, $B = 0.2$, (j) inlet Position A, $B = 0.5$,
 (k) inlet Position A, $B = 0.8$

Effect of blocking position on outlet velocity

Figure 10 shows the velocity cloud diagram of the cross-section of flow channel on the axis of the blocking hole. When the blocking ratio $B = 0.8$, the area of air film perpendicular to the blade surface at temperatures from 1100-1240 K is significantly reduced compared with that without blocking. The blockage changes the direction and size of the air velocity at the outlet of the hole, which has a great influence on the cooling efficiency of the air film. As a result, in the same position, with the increase of the blocking ratio, the outlet flow of the air film hole will gradually become smaller due to high temperature mainstream air mixing, resulting in shorter acting distance of the cooling fluid-flowing out of the air film hole, which is most obvious in inlet Position A.

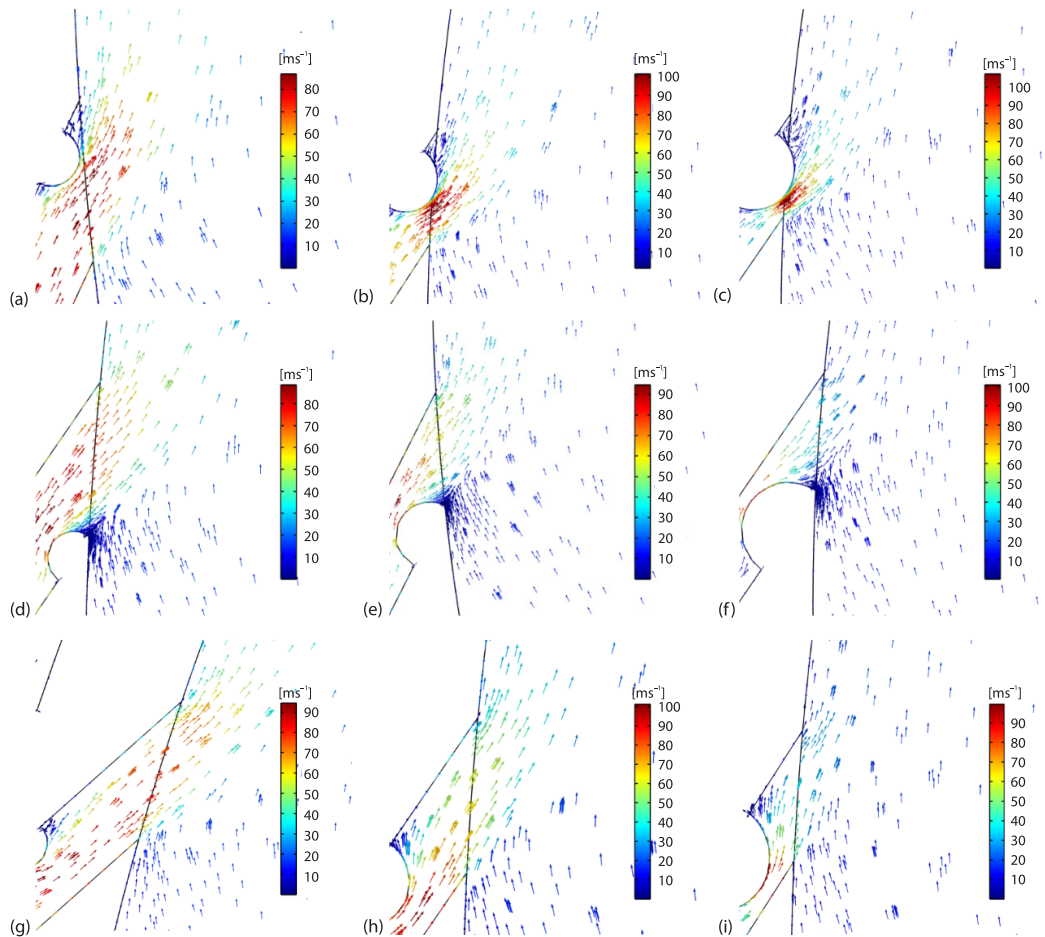


Figure 10. Velocity cloud of flow cross-section on the axis of blocking hole;
 (a) outlet Position 1, $B = 0.2$, (b) outlet Position 1, $B = 0.5$, (c) outlet Position 1, $B = 0.8$,
 (d) outlet Position 2, $B = 0.2$, (e) outlet Position 2, $B = 0.5$, (f) outlet Position 2, $B = 0.8$,
 (g) inlet Position A, $B = 0.2$, (h) inlet Position A, $B = 0.5$, and (i) inlet Position A, $B = 0.8$

It is found that for the same blocking ratio, the angle between the high temperature mainstream and the cooling fluid in different positions is shown outlet Position 1 > outlet Position 2 > inlet Position A. In inlet Position A, when the blockage ratio $B = 0.8$, the cooling

fluid-flow rate at the outlet of the air film hole is significantly reduced, the angle between the high temperature mainstream and the cooling fluid is the smallest, and the resistance between the cooling fluid and the high temperature mainstream is the weakest, resulting in the smallest covering area of the air film on the blade surface.

Test on effect of air film coverage

Section *Test on effect of air film coverage* mainly focuses on the test on effect of cooling fluid coverage of the first stage HPT blade of PW4084 aviation engine. Section *Test on effect of air film coverage* provides a detailed introduction the experimental model, experimental equipment, and experimental results. Based on the experimental parameters, the model is constructed and analyzed in accordance with the previous numerical model for air film cooling to verify the reliability of the numerical model proposed earlier in the paper. In this experiment, water is used as the cooling fluid due to difficulty in controlling and observing the air.

Blade for testing

The experiment uses the first stage HPT blade of the Pratt and Whitney PW4084 aircraft engine used in the previous modelling as the research object. The experimental blade model is shown in fig. 11, which is consistent with the 3-D model used in the previous numerical model. This experiment only measures the effect of cooling fluid coverage on the pressure surface of the blade without considering the effect of cooling fluid coverage on the suction surface and the top transverse exhaust film hole.

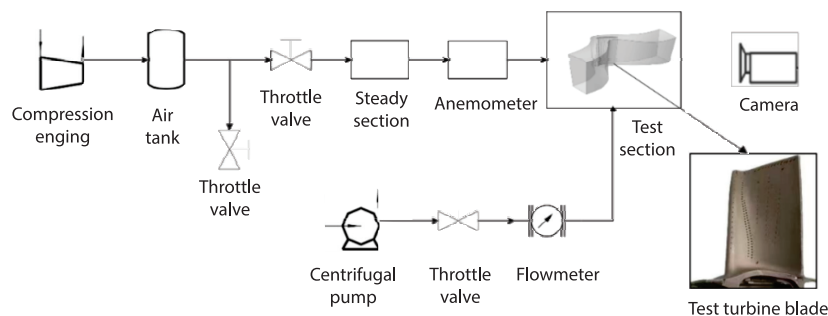


Figure 11. Test system flow diagram

Test system

The experimental system mainly consists of a water supply system, an air supply system, a measuring device, and an experimental section as shown in fig. 12. In this experiment, the water supply system provides cooling fluid for a self-priming booster pump, with a rotational speed of 2860 rpm and maximum flow rate of 4.8 m³ per hour. The cooling fluid is connected through a pipe-line and entered the interior of the blade for testing. The mainstream air supply system is provided by an air compressor, which can provide a maximum volume flow rate of 0.18 m³ per minute and a maximum exhaust pressure of 1.5 MPa. The air-flow is sent to the mainstream channel through a pipe-line to simulate mainstream impact. The measuring device consists of a wind speed measuring device and a camera. The range of the anemometer is 0~70 m/s as shown in fig. 12(a). The experimental section mainly consists of the mainstream channel and blade clamping device, and the inlet size of the mainstream channel is length × width = 100 × 60 mm, and the outlet size is also length × width = 100 × 60 mm, the shape of the main flow channel refers to the mainstream channel model used in the prior

simulation, and slight adjustments are made in accordance with the processing situation. A small wind speed stabilizing device is installed in front of the mainstream channel inlet to ensure that the mainstream impact the blades with stable wind speed as shown in fig. 12(b). The blade clamping device is made of aluminum, and the size of the clamping device is length \times width \times height = 66 \times 66 \times 150 mm, with the upper part being the blade clamping device and the lower part being the cooling fluid inlet. The inlet and clamping device are connected with bolts and sealed with rubber gaskets. Figures 12(c) and 12(d) present the blade clamping device sealed with a sealant, which is used to ensure an even flow of cooling fluid into the interior of the blade.

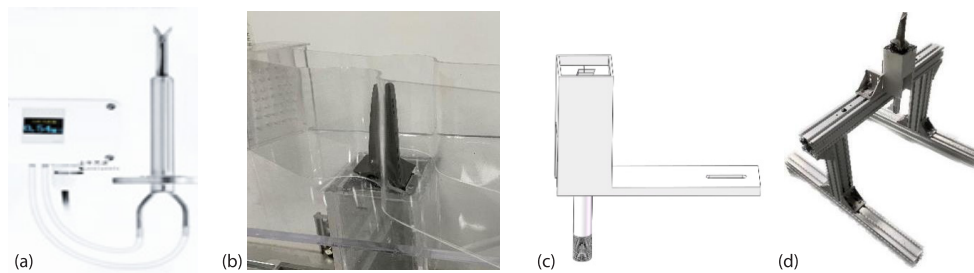


Figure 12. Test device; (a) measurement device, (b) mainstream channel, (c) clamping device model, and (d) clamping device

Analysis of experimental errors

Affected by many factors in the experiment, the errors between the data and the actual objective values are inevitable. To address these errors, the following measures should be taken:

- Before the experiment, calibrate the speed measuring device and debug the testing equipment to ensure that the equipment is in good operating condition.
- During the installation of the specimen, a standardized process is applied to check the airtightness of the pipe-line and ensure a stable supply of cooling fluid and mainstream.
- During the experiment, environmental factors such as temperature and atmospheric pressure should be recorded and their impact on the test results should be reduced to the minimum.
- During the experiment, minimize human interference such as operational errors, *etc.*
- When comparing and analyzing data, it is essential to take into account differences in experimental conditions and uncertainty of results, and to avoid over-interpretation and generalization of experimental results.

Numerical simulation

The numerical calculation model remains the same as the experimental blade parameters, and all boundary conditions remain except for the cooling fluid converted from air to water. The specific parameters are shown in tab. 4. The calculation model grid is generated with a simulation software grid generator and encrypted on the blade surface and cooling channel wall. The total number of grids is 3 million as shown in fig. 13.

Table 4. Test and simulation parameters

	Mainstream	Jet
Temperature	295 K	293 K
Velocity	30 m/s	2.95 m/s

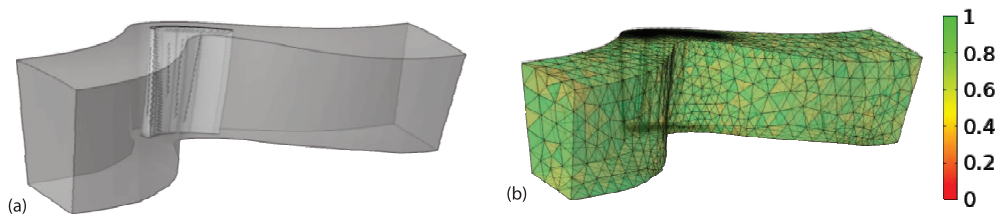


Figure 13. Computational numerical model;
(a) computational numerical model and (b) grid division

Comparison of test results

Figure 14 exhibits the experimental and numerical simulation results for mainstream speeds of 0 m/s and 30 m/s, respectively. As shown in fig. 14, the test results show that on the pressure surface, when the mainstream wind speed is 0 m/s, the cooling fluid-flows out of the air film hole and shoots straight back along the direction of the air film hole. The velocity direction of cooling fluid is along the direction of the air film hole, and the cooling fluid cannot form an effective film on the surface of the blade. When the mainstream flow velocity is 30 m/s, the cooling fluid-flows out of the air film hole and it can cover the surface of the blade to form an effective film and extend backwards under the high speed mainstream action. Under the mainstream action, the originally irregular flow of the cooling fluid becomes uniform, especially in the holes near the edge of the blade where the cooling fluid is evenly distributed and flows backwards.

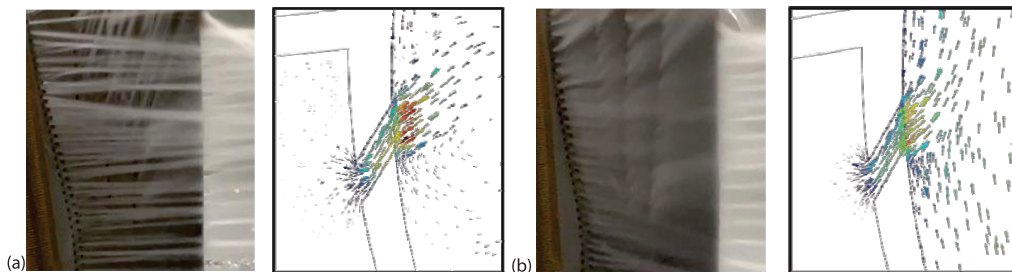


Figure 14. Test and simulation results; (a) wind speed in the main channel is 0 m/s and
(b) wind speed in the main channel is 30 m/s

The simulation results present that on the pressure surface, when the mainstream wind speed is 0 m/s, the cooling fluid-flows out of the air film hole and deflects in the direction of the cooling fluid velocity along the air film hole and keeps away from the blade surface. The cooling fluid cannot form an effective air film on the blade surface, which is consistent with the experimental results. The outward deflection is due to the small size of the simulated mainstream flow channel, and the cooling fluid will form eddies in the mainstream flow channel without the influence of the mainstream, affecting the direction of cooling fluid deflection. When the mainstream speed is 30 m/s, compared to 0 m/s, the cooling fluid-flow direction bends towards the blade surface under the high speed mainstream effect and forms an effective film covering the blade surface, which is basically consistent with the experimental results. As shown in fig. 15, air film effect experiment when the mainstream wind speed is 30 m/s and the bottom four holes of the third column of the pressure surface are blocked. In accordance with the experimental results, when the air film hole is completely blocked, the covering effect of

the cooling fluid near the area behind the air film hole changes little. As the cooling fluid gradually diffuses backward, the air film hole is blocked, resulting in a decrease in the flow rate of the cooling fluid, a decrease in the air film area covered by the blade surface, and a decrease of the cooling efficiency.

Conclusions

After conducting the simulation, different blocking ratios of local air film holes in blades were studied. Modelling of different blockage states of air film holes in typical positions is used to analyze the changes of air film cooling efficiency, temperature field and flow field. The effect of local blockage on air film flow field is further explored through experiments. The specific conclusions are as follows.

- The air film cooling efficiency on the downstream region of the exit of the air film holes decreases due to the blockage, and the decreasing amplitude increases non-linearly. The blockage of the air film holes changes the state of the flow field where the protective air film is formed, shortening the protective distance of the cooling air. With the increase of the blocking ratio, a large-scale asymmetric reverse vortex is formed on the blade surface. This factor makes the blade surface carry more hot air from the mainstream, prompts the cooling air film to move away from the blade surface, and facilitates the mixing of the cooling flow field with mainstream. Eventually, the cooling efficiency of the air film decreased.
- For $x/d = 1$ and blocking rates $B \leq 0.2$, the fluctuations of cooling efficiency of air film remain less than 2% in spite of different blocking positions. With the increase of the blocking ratio, the influence of the blocking in inlet position A on the cooling efficiency of the air film becomes increasingly apparent. When $B = 0.8$, the decreasing amplitude reaches to 7.29%. In the $x/d = 4$ region of downstream of the blocking hole, the blockage in these three positions significantly reduces the cooling efficiency of the air film, and the decreasing amplitude is close. However, when $B = 0.2$, the influence of the three blocking states on the cooling efficiency exceeds 6%, and when $B = 0.8$, the cooling efficiency decreased by over 10%. The comprehensive results show that when the blockage is in inlet Position A, it has the greatest influence on the cooling efficiency of the air film.
- The cross-section of the air film formation flattens out in the downstream region of the air film holes where the temperatures are lower than 1100 K and in the same position of the blockage. This factor results in lower air film thickness with increasing blockage ratio. In inlet position A, when the blocking ratio $B = 0.8$, the blocking condition makes the direction of the cooling air film convert to that of the high temperature mainstream, and the effective protective air film is the smallest.
- With the same blocking ratio, different blocking position, respectively matches different angle between the high temperature mainstream and the cooling fluid, thus the angle in outlet Position 1 > outlet Position 2 > inlet Position A. In inlet Position A, and when the blockage ratio $B = 0.8$, the cooling fluid-flow rate at the outlet of the air film hole decreases significantly, the angle between the high temperature mainstream and the cooling fluid is the smallest, and the formed resistance is the weakest, these three factors result in the smallest covering area of the air film on the blade surface.

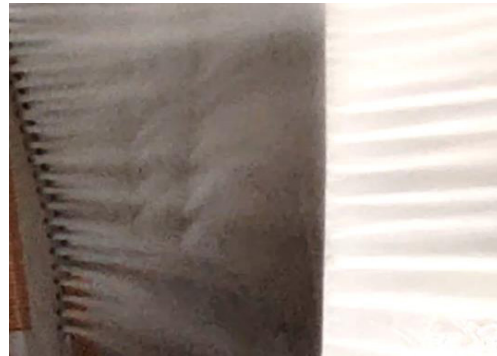


Figure 15. Effect of local blockage coverage

- The experimental results show that when the air film hole is unblocked and the wind speed of mainstream on the pressure surface is 0 m/s, the cooling fluid-flows out along the direction of the air film hole without forming protective air film. After flowing out of the air film holes, 30 m/s mainstream makes the cooling fluid cover the blade surface so as to form an effective film. In the condition of several air film blocked, the flowing speed, flowing direction and coverage rate change, and the changing trends of these three factors are consistent with those of numerical analysis.

Acknowledgment

The authors acknowledge the financial supports by the Fundamental Research Funds for the Central Universities of Civil Aviation University of China (No. 3122023043).

Nomenclature

d	– diameter of the air film hole, [mm]
\mathbf{F}	– force vector, [N]
p	– pressure, [Pa]
Q	– contained in other reservoirs, [W/m ³]
Q_{ted}	– thermoelastic damping heat source, [W/m ³]
Q_{urb}	– turbulent heat flux, [W/m ³]
Q_{vd}	– viscous dissipative term (in fluid mechanics), [W/m ³]
\mathbf{q}	– conduction heat flux, [W/m ²]
\mathbf{S}	– strain rate tensor, [–]
T	– temperature, [K]
\mathbf{u}	– velocity vector, [ms ⁻¹]
v	– velocity, [ms ⁻¹]

Greek symbols

ρ	– density, [kgm ⁻³]
$\boldsymbol{\tau}$	– radiant heat flux, [Wm ⁻²]
μ	– dynamic viscosity, [kgm ⁻¹ s ⁻¹]

Subscripts

aw	– adiabatic surface of the blade
c	– mainstream
g	– jet

References

- [1] Mu, X., *et al.*, A New Assembly Precision Prediction Method of Aeroengine High-Pressure Rotor System Considering Manufacturing Error and Deformation of Parts, *Journal of Manufacturing Systems*, 61 (2021), Oct., pp. 121-124
- [2] Wang, J., *et al.*, Effects of Hole Configuration on Film Cooling Effectiveness and Particle Deposition on Curved Surfaces in Gas Turbines, *Applied Thermal Engineering*, 190 (2021), 116861
- [3] Kim, J., *et al.*, Deposition of Volcanic Materials in the Hot Sections of Two Gas Turbine Engines, *Journal of Engineering for Gas Turbines and Power*, 115 (1993), 3, V003T05A001
- [4] Liu, Z., *et al.*, An Experimental Study of the Effects of Different Transverse Trenches in Deposition on a Turbine Vane with Film-Cooling at High Temperature-ScienceDirect, *Aerospace Science and Technology*, 88 (2020), 5, pp. 40-50
- [5] Yu, K., Tuffyti, D. K., Size and Temperature Dependent Collision and Deposition Model for Micronsized Sand Particles, *Journal of Turbomachinery*, 141 (2018), 3, 031001
- [6] Chen, X., *et al.*, Effect of Particle Deposition on Film Cooling from Fan-Shaped Holes, *International Journal of Heat and Mass Transfer*, 181 (2021), 181, 122028
- [7] Chen, X., *et al.*, Large Eddy Simulation of Film Cooling from Cylindrical Holes Partially Blocked by CaO-MgO-Al₂O₃-SiO₂, *International Communications in Heat and Mass Transfer*, 129 (2021), 129, 105754
- [8] Li, G., *et al.*, Effect of Hole Blockage on the Film Cooling Effectiveness of a Blade on the Suction Side, *Journal of Engineering for Thermal Energy and Power*, 36 (2021), 311, pp. 41-46 + 56
- [9] Huang, K., *et al.*, Effect of Partial Blockage Inside Film Hole on Film Cooling Characteristics, *Journal of Aerospace Power*, 29 (2014), 06, pp. 1330-1338
- [10] Zhou, J., Zhang, J., Effect of Local Blockage of Film Holes on the Integrated Cooling Efficiency of Blade Pressure Surface Impingement Spoiler Film Structure, *Acta Aeronautica ET Astronautica Sinica*, 37 (2016), 09, pp. 2729-2738
- [11] Pu, J., *et al.*, Numerical Investigation of Effects of Blockage, Inclination Angle, and Hole-Size on Film Cooling Effectiveness at Concave Surface, *Journal of Turbomachinery*, 143 (2021), 2, pp. 1-59

- [12] Sundaram, N., Thole, K., Effects of Surface Deposition, Hole Blockage, and Thermal Barrier Coating Spallation on Vane Endwall Film Cooling, *Journal of Turbomachinery*, 129 (2007), 7, pp. 599-607
- [13] Yang, X., et al., An Experimental Study on Turbine Vane Leading-Edge Film Cooling with Deposition, *Applied Thermal Engineering*, 198 (2021), 117447
- [14] Guo, Y., et al., Effect of Film Hole Blockage on Film Cooling on Blade Suction Surface, *Journal of Power Engineering*, 41 (2021), 01, pp. 28-35
- [15] Whitfield, C. A., et al., Blockage Effects from Simulated Thermal Barrier Coatings for Cylindrical and Shaped Cooling Holes, *Proceedings, ASME Turbo Expo: Turbine Technical Conference and Exposition*, American Society of Mechanical Engineers, Dusseldorf, Germany, 2014
- [16] Wei, J., et al., Effectiveness of Impinging-Film Cooling for Different Inducting S-Labs, *Heat Transfer Research*, 50 (2019), 13, pp. 1285-1305
- [17] Zhang, W., et al., Effect of Blockage Inside Holes on Film Cooling Performance on the Suction Side of a Turbine Guide Vane, *Energies*, 15 (2022), 8, 2935
- [18] Tian, K., et al., Effect of Blockage Configuration on Film Cooling with and without Mist Injection, *Energy*, 153 (2018), 15, pp. 661-670
- [19] Sundaram, N., Thole, K. A., Effects of Surface Deposition, Hole Blockage, and Thermal Barrier Coating Spallation on Vane Endwall Film Cooling, *Journal of Turbomachinery*, 129 (2007), 3, pp. 599-607
- [20] Wang, J., et al., Effect of Spherical Blockage Configurations on Film Cooling, *Thermal Science*, 22 (2018), 5, pp. 1933-1942
- [21] Chen, X., et al., Influence of Conjugate Heat Transfer Performance of Film Cooling on CMAS Particle Deposition, *Thermal Power Engineering*, 36 (2021), 10, 10
- [22] Huang, K., et al., Experimental Study on Film Cooling Performance of Imperfect Holes, *Chinese Journal of Aeronautics*, 31 (2018), 6, pp. 1215-1221
- [23] Jovanovic, M. B., et al., Influence of Laser Drilling Imperfection on Film Cooling Performances, *Proceedings, ASME Turbo Expo 2005: Power for Land, Sea, and Air*, Reno, Nev., USA, 2005, Vol. 3, 11, pp. 285-292
- [24] Jovanovic, M. B., et al., Influence of Hole Imperfection on Jet Cross-Flow Interaction, *International Journal of Heat and Fluid-Flow*, 27 (2006), 1, pp. 42-53
- [25] Jovanovic, M. B., et al., Effect of Hole Imperfection on Adiabatic Film Cooling Effectiveness, *International Journal of Heat and Fluid-Flow*, 29 (2008), 2, pp. 377-386
- [26] Mahesh, K., The Interaction of Jets with Crossflow, *Annual Review of Fluid Mechanics*, 45 (2013), 1, pp. 379-407
- [27] Gong, M., et al., Film Cooling Mechanism and Flow Field Analysis of Turbine Blade Leading Edge, *Journal of Weapon Equipment Engineering*, 43 (2022), 09, pp. 232-239
- [28] Demling, P., Bogard, D. G., The Effects of Obstructions on Film Cooling Effectiveness on the Suction Side of a Gas Turbine Vane, *Proceedings, ASME Turbo Expo 2006: Power for Land, Sea, and Air*, Barcelona, Spain, 2006
- [29] Huang, K., et al., Effect of Partial Blockage Inside Film Hole on Film Cooling Characteristics (in Chinese), *Journal of Aerospace Power*, 29 (2014), 06, pp. 1330-1338